Quantitative Phase Imaging (QPI) in Neuroscience

Chenfei Hu and Gabriel Popescu

(Invited Paper)

Abstract—Quantitative phase imaging (QPI) is an emerging label-free modality that attracts significant interest in biomedicine in general and neuroscience in particular. Based on the principle of interferometry, QPI precisely maps the optical pathlength induced by the sample, and, thus, can visualize extremely transparent samples. The QPI field has grown rapidly in the past decade, and reliable instruments have been developed for in-depth biological studies. One particular figure of merit associated with QPI techniques describes the temporal phase sensitivity of instruments. Recently, several common path interferometry methods have been developed, which yield high stability and nanometer scale pathlength sensitivity. In neuroscience, QPI has shown unique capabilities in quantifying neural growth and dynamics in cell cultures, as well as high contrast imaging of brain tissue slices. In this paper, we review the principles of QPI, novel QPI technology, advances in data processing, and a number of exciting applications in neuroscience.

Index Terms—Biomedical optical imaging, microscopy, phase measurement, neuroscience, quantitative phase imaging.

I. INTRODUCTION

THE phase change of an optical field as it interacts with a specimen is a valuable contrast mechanism, as it allows the study of unlabeled transparent specimen [1]. Zernike's phase contrast microscope uses these phase differences to visualize fine structures in weakly absorption objects, without exogenous labeling [2], [3]. Gabor proved later the possibility of storing complex field information, which can be subsequently used to reconstruct the image of an object of interest [4], [5]. Built upon these pioneering ideas, quantitative phase imaging (QPI) emerges as an exciting imaging modality that accurately reports on both the thickness and the refractive index of the sample of interest. Over the past decade, a number of novel QPI platforms were developed to improve the resolution and sensitivity both in time and space, which enable a range of applications, from dynamics of single cells, medical diagnosis, and neuroscience studies [6]–[11]. In this article, we review the progress of QPI instruments, and recent applications in neuroscience.

II. QPI PRINCIPLE

In a typical transmission microscopy system, the image field as a function of space and time can be expressed as

$$U_i(x,y,t) = |U_i(x,y)|\, e^{-i[\langle\omega\rangle t - \langle\mathbf{k}\rangle\cdot\mathbf{r} + \varphi(x,y)]} \tag{1}$$

In Eq. 1, $|U_i(x,y)|$ the magnitude of the field, $\langle\omega\rangle$ the central frequency, $\langle\mathbf{k}\rangle$ the central wavevector, $\mathbf{r}$ the spatial coordinates, $\varphi(x,y) = \frac{2\pi}{\lambda}[\bar{n}(x,y) - n_0]h$ is the phase of the interest [12], λ the central wavelength, $\bar{n}$ the axial average refractive index across the field of view (FOV), n_0 the background refractive index, and h the thickness of the interest of study. A conventional photodetector is only sensitive to the intensity of the field, i.e., the modulus squared of the field is obtained. QPI is essentially interested in extracting φ and it borrows ideas from interferometry and holography to achieve this goal. In QPI, a reference field, U_R, is introduced to mix with image field, and, as a result, the camera detects the interference of the combined field, which is written as

$$\begin{aligned} I(x,y,t) = & |U_i(x,y)|^2 + |U_R|^2 \\ & + 2|U_i(x,y)|\,|U_R|\cos[\langle\omega\rangle(t - t_R) \\ & - (\langle\mathbf{k}\rangle - \mathbf{k_R})\cdot\mathbf{r} + \varphi(x,y)] \end{aligned} \tag{2}$$

where t_R and $\mathbf{k}_R$ are the time delay and wavevector associated with the reference field, respectively, composing the two main QPI configurations, as follows. Off-axis QPI system uses a $\mathbf{k}_R$ different than the direction of image filed, while the phase-shifting QPI modulates the t_R (Fig. 1). The methods of obtaining φ are discussed below.

In off-axis geometry, the sample and slightly tilted reference fields go through different paths and recombine at the image plane and form an interferogram on the detector (Fig. 1a). The spatial irradiance associated with the interferogram, $I(x, y)$, is given by

$$\begin{aligned} I(x,y) = & |U_i(x,y)|^2 + |U_R|^2 \\ & + 2|U_i(x,y)|\,|U_R|\cos[\Delta kx + \varphi(x,y)] \end{aligned} \tag{3}$$

where $\Delta k = |\langle\mathbf{k}\rangle - \mathbf{k}_R|$ is the magnitude of the wavevector difference between the image and reference field, which is assumed to be along the x-axis and acts as the carrier frequency. After isolating the cosine term from the raw interference using the Fourier transform, the corresponding sine component can be calculated via a Hilbert transform, as

$$\sin[\Delta kx + \varphi(x,y)] = P\int\frac{\cos[\Delta kx' + \varphi(x,y)]}{x - x'}dx'. \tag{4}$$
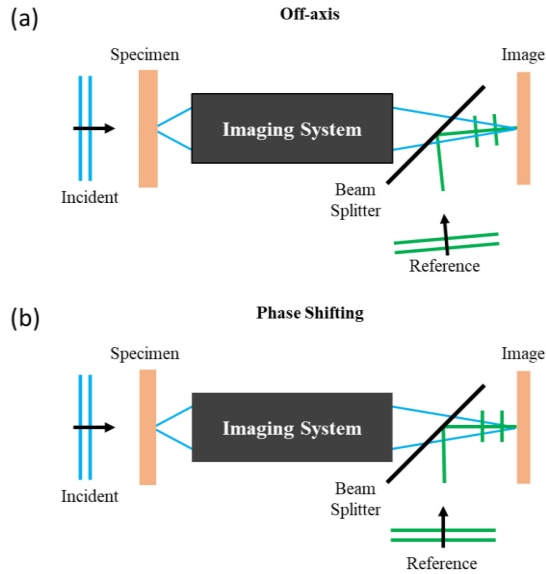
Fig. 1. Two main QPI configurations. (a) Off-axis tilts the propagation axis of the reference field to produce an interference pattern so that the phase shift due to the specimen is obtained from a single image. (b) In Phase shifting QPI, the reference field propagates along the same axis as the object field. The phase of the reference field is successively shifted by $\pi/2$ to produce four images, which are combined to extract the phase shift induced by the specimen.

As a result, $\Delta kx + \varphi(x, y)$ is extracted from the complex analytical field, $\exp[i(\Delta kx + \varphi(x, y))]$. The phase map of interest, φ, is eventually retrieved by subtracting Δkx, which is the tilted plane with a slope of Δk. As one can see, off-axis method reconstructs a phase map from one raw measurement, therefore, in theory, the speed of this imaging modality is only limited by the photodetector.

By using a translating mirror or other mechanisms to introduce additional phase delay between sample and reference light, phase-shifting type of QPI records a collection of images to retrieve the associated phase (Fig. 1b). The image irradiance at the camera takes the form as

$$I(x, y, \delta) = |U_i(x, y)|^2 + |U_R|^2$$
$$+ 2|U_i(x, y)||U_R| \cos[\varphi(x, y) + \delta] \quad (5)$$

where $\delta = \langle\omega\rangle(t - t_R)$. Using a modulated phase delay, each with an increment of $\pi/2$, a phase map can be reconstructed from a collection of 4 intensity images,

$$\varphi(x, y) =$$
$$\arctan 2 \left[I(x, y; 0) - I(x, y; \pi), I\left(x, y; -\frac{\pi}{2}\right) - I\left(x, y; \frac{\pi}{2}\right) \right]. \quad (6)$$

In Eq. 6, arctan2 is a Matlab syntax as the *argument* function, which is defined as

$$\arctan 2(x, y) = \begin{cases} \arctan(y/x), x > 0 \\ \pi/2, x = 0, y > 0 \\ -\pi/2, x = 0, y > 0 \\ \pi + \arctan(y/x), x < 0, y < 0 \end{cases} \quad . \quad (7)$$

From another point of view, light traveling path is another way to categorize QPI systems. In common-path methods, as
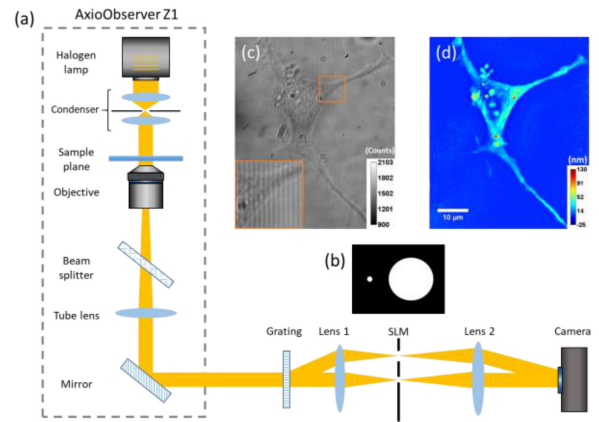
Fig. 2. Schematic of DPM. (a) DPM is off-axis, common-path module attached to a conventional bright-field microscope. (b) The sample and reference field is created by spatial filtering at the Fourier plane. (c) A raw interferogram and (d) its corresponding optical pathlength map. Adapted with permission from Ref. [15].

oppose to non-common path, the sample and reference fields propagate in the same optical path or in vicinity to each other. The two interference beams experience the same disturbance in background, and as a result, the background noise is greatly canceled out in the measured interferogram, which significantly improves the temporal-phase stability.

III. RECENT ADVANCES IN INSTRUMENTATION

A. Off-Axis Methods

One of the early demonstrations of common-path, off-axis QPI is called diffraction phase microscopy (DPM), which is realized by attaching an additional module to the camera port of an existing microscope system (Fig. 2) [13]. At the output of a bright-field microscope, a transmission grating is placed at the image plane, and then multiple diffraction orders are produced with each containing the full spatial information about the sample. All diffraction orders are blocked, except the 0th and 1st order beam. At the Fourier plane, using a physical pinhole or a spatial light modulator (SLM), one diffraction beam is spatially low passed to create a DC reference field, while it leaves the other beam intact to form the sample field (Fig. 2b). After the second Fourier lens, the two beams recombine and form an interferogram on the detector, where the fringes, in some level, are perturbed by the phase delay of the interest (Fig. 2c). Finally, a phase map is reconstructed as shown in Fig. 2d [14].

Depended on the illumination power and the detector quality, this system can run as fast as several hundred frames/second. In authors' lab, by incorporating CUDA parallel computing architecture, a real-time DPM reconstructing and displaying system was demonstrated, which achieved a speed as fast as 40 frames/s [16]. In addition, this stand-alone module is also compatible with reflection measurement, which enables imaging topological structures of reflective surfaces, such as semiconductors [17]–[19]. Finally, by modulating the wavelength of illumination, spectroscopic off-axis method has the potential of providing chemical or functional information about the specimen [20]–[22].
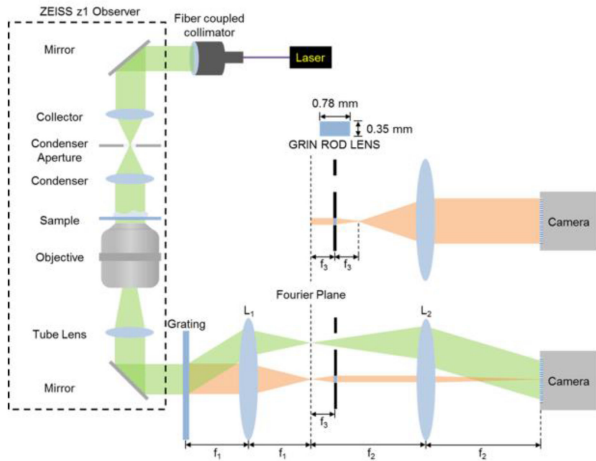
Fig. 3. Schematic of a MISS module. MISS utilizes a GRIN lens to produce a magnified image of 0th diffraction beam. And the reference field fully covers the camera plane. Adapted with permission from Ref. [23].

Fig. 4. System schematic of SLIM. The SLIM module, outside of a phase contrast microscope, provides additional phase delay between scattered and unscattered light. As a result, 4 intensity images with different phase delay are collected to produce one correspond quantitative phase image. Adapted with permission from Ref. [26].

Fig. 5. Principle of GLIM. (a) GLIM works as an add-on module attached to the output of a DIC microscope. The SLM unit shifts the phase of one polarization component, while the other remains intact. (b) 4 intensity images, each with different phase delay, are recorded, and a quantitative phase gradient map is extracted in (c). Adapted with permission from Ref. [27].

Built upon the principle of DPM, a magnified image spatial spectrum (MISS) microscopy technique was recently invented [23], which further pushes the limit of the imaging speed. Figure 3 shows the schematic of the MISS module. Instead of using a pinhole, MISS adapts a gradient index (GRIN) lens, L_3, with a very short focal length to manipulate the 0th diffraction beam, where the Fourier plane is located at the GRIN lens's front focal plane. L_3 and L_2 form another 4-f system and enlarge the image of 0th diffraction beam with a magnification factor of 500, and this makes the camera only detects the DC component of the 0th order beam as the reference field. In other words, the camera itself plays the role of a low-pass filter, which eliminates the necessity of aligning the micrometer-size pinhole. Furthermore, the authors show that MISS design provides comparable performance to a DPM system, but can run at a speed as fast as 833 frame/s, making it possible to study fast dynamic phenomena in live samples.

B. Phase-Shifting Methods

Spatial light interference microscopy (SLIM) [24], [25] is a typical common-path, phase-shifting QPI system. Based on an existing Zernike microscope, SLIM combines the phase contrast method by revealing intrinsic contrast of transparent samples, with Gabor's holography by obtaining quantitative phase value across the sample. A system schematic of SLIM is shown in Figure 4. At the output of a phase contrast microscope, two Fourier Lens, L1 and L2, compose a 4-f system and relays the image plane to the CCD deter plane. A liquid crystal phase modulator (LCPM) is placed at the back focal plane of L1 to provide additional phase shift between scattered (sample) field and unscattered (reference) field, by increments of $\pi/2$. The projected pattern on LCPM is precisely calculated to match the size and position of the phase ring in the objective. As a result, 4 intensity images, each with a different delay, are acquired, and then the phase delay is uniquely determined using Eq. 6. Employing a broadband white light as the illumination source, SLIM provides speckle-free phase maps, with exceptional high sensitivity and stability. Unlike DPM using grating to produce interferograms,
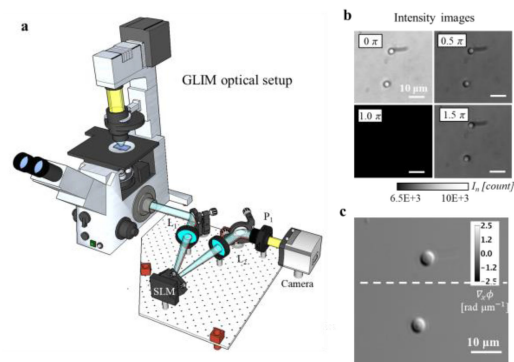
SLIM enables multimodal investigation (including fluorescent) by switching different LCPM patterns.

More recently, a novel label-free method, referred to as gradient light interference microscopy (GLIM), has been developed in authors' lab [27]. Instead of using a Zernike microscope, GLIM combines the differential interference contrast (DIC) microscopy with low coherence microscopy and holography (Fig. 5). In GLIM, the two interfering fields are identical except for a small transverse shift. This geometry ensures that the two fields suffer equal degradation due to multiple scattering. By accurately controlling the phase shift between the two waves, 4 intensity images are obtained, each containing same phase information but a different phase delay. As a result, GLIM produces a clear gradient phase map that rejects much of multiple scattering, which is suitable to image thick samples. Furthermore, using fully open condenser, GLIM proves it strong sectioning and resolution capabilities.

IV. APPLICATIONS

Accompanied by the advances in system design, QPI field rapidly grows and it has become a remarkable imaging modality, especially suitable to study biological samples. Due to its

capabilities of label-free imaging, high sensitivity and stability, and quantitative information, it can be used to probe the structures and functions at different levels. In addition, researchers came up with a number of data analyzing methods, which extract a few quantities from phase maps to provide insightful knowledge of the sample of interest. With the combination of QPI platform and proper analyzing methods, this imaging techniques has shown its power in a number of studies, such as cellular dynamics [28], [29], cell growth & proliferation [30]–[32], mass transport [33], cell-substrate interaction [34], impact of extracellular environment [35], [36], and pathological applications [37]–[40]. Recently, authors' group, along with other research groups, have translated QPI to neuroscience studies [41]. Traditionally, a neuroscientist uses electrophysiological methods or fluorescent imaging to study a specimen. Though electrophysiology methods provide high fidelity readout of neural activity, the low spatial throughput limits its capability of investigating intra- and inter- cellular interactions of individual neuron among the network [42]. On the other hand, by introducing a fluorescent sensor, optical imaging can provide functional information, even electrical activity in both a single neuron and a network [43]–[45]. But this process requires careful sample preparation, and it is not suitable for long term imaging due to photo-toxicity and photo-bleaching [46]. Here we report a few examples where QPI open a unique avenue to address questions in neuroscience.

A. Growth of Neuronal Network

The development of neuronal network in general is a complex process. A single nerve cell, called neuron, detects a variety types of stimulants both inside and from the medium, gradually organizes into groups, and forms units with specific functions.

Using QPI, one would be able to measure a forming neural network at multiple temporal and spatial scales, in a high throughput and minimally invasive manner. Moreover, the quantitative phase value is proportional to non-aqueous content in the cell, also called dry mass, which enables studying the growth of cell bodies, extensions of neurites, changes of cell populations. According to the literature, the refractive index properties of the cell, n_c, show a linear dependence on the total cell protein concentration [47]

$$n_c(x, y) = n_0 + \alpha C(x, y) \qquad (8)$$

where n_0 the refractive index of the water, C is the concentration of non-aqueous content of the cell (unit: g/ml), α the refraction increment (unit: ml/g). The total dry mass of the cell is the integrated phase value over the cell surface area, then scaled by the constant

$$M = \iint_A \sigma(x, y)\, dx dy$$

$$= \frac{\lambda}{2\pi\alpha} \iint_A \varphi(x, y)\, dx dy. \qquad (9)$$
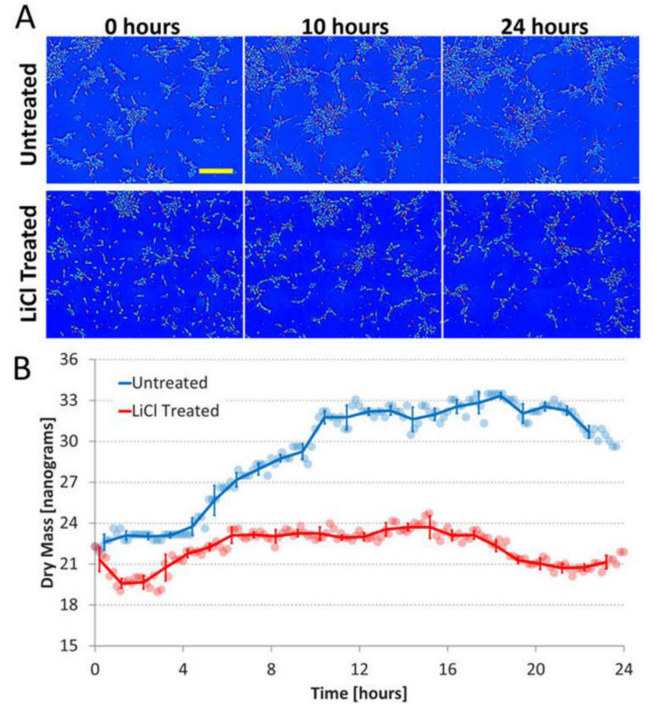
Fig. 6. Label-free investigation of forming neuronal network. (a) Dry mass density maps acquired at 0, 10, and 24 hours for both the untreated and LiCl treated cultures; the yellow scale bar corresponds to 200 μm. (b) Total dry mass vs. time of the entire field of view for both conditions. Adapted with permission form Ref. [48].

One example of this application is shown in Fig. 6, where researchers used SLIM to observe the emerging process of neuronal network at a large FOV [48]. In this research, two different differentiated human neuronal cell cultures were imaged for a period of 24 hours. 15 mM LiCl was added to the medium of one cell culture to retard neurite outgrowth as the experiment group. The dry mass of the measured area at each time point was calculated and plotted (Fig. 6b). Their results show that increased neuron population as well as connected networks appeared in the untreated group after 24 hours, as contrary to the LiCl treated group, where cells mostly stayed in isolated clusters (Fig. 6a). When looking at the dry mass change, drastic difference can be observed between the experiment and control group. Also, even for the untreated group, Fig. 6b reveals different type of growth features at different time period, which suggest a correlation between protein production and network structures. Similar to the result of another study in Ref. [26], where Cintora *et al.* measured the rate of dry mass change of neuron culture in low, medium, and high-confluence conditions for a time course approximately 30 hours (Fig. 7), the authors also found that neurons tend to produce less mass in higher confluence regions.

B. Mass Transport

Dispersion-relation Phase Spectroscopy (DPS) is a QPI data analyzing tool for describing how mass is transported inside or between live specimens. DPS uses a time-stack phase video as input, and extracts diffusion coefficient as well as the bandwidth
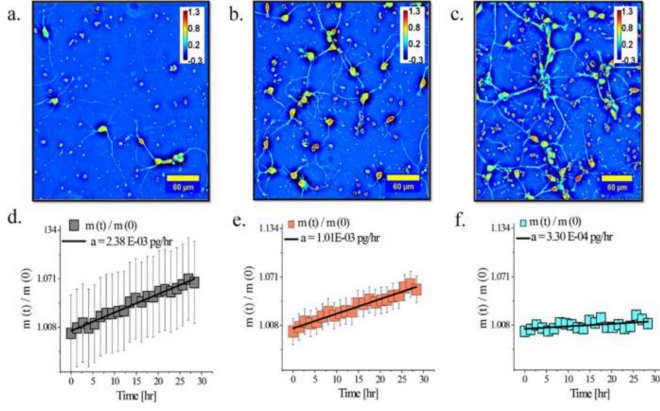
Fig. 7. Quantitative assessment of neuronal growth. (a-c) SLIM images representing low, medium and high confluency conditions, respectively, and (d-f) the corresponding total dry mass change over a time course of 30 hours. Adapted with permission from Ref. [26].
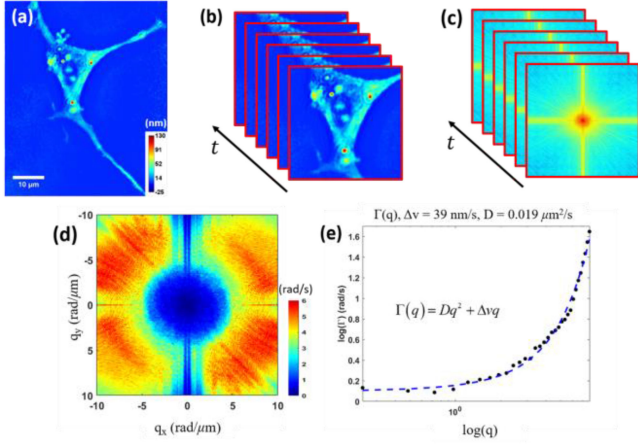
Fig. 8. Procedure of DPS. After the measurement, a region of interest (ROI) in the field of view is selected(a), and the image volume is digitally aligned to minimize drifts between frames (b). Taking a Fourier transform on each frame (c), the temporal bandwidth is then evaluated and obtain map of Γ(d). Performing a radial average on (d), the advection and diffusion coefficients are extracted from dispersion curve(e). Adapted with permission from Ref. [15].

of advection velocity, without the need of tracking individual particles. This procedure is briefly described here (Fig. 8), and more detailed discussion of the theory are included in Ref. [49]. For a given QPI time-stack, each frame, φ, is essentially proportional to dry mass density (Fig. 8a, b), it is assumed to satisfy the diffusion-advection equation, namely [49]

$$D\nabla^2\varphi(\mathbf{r}, t) - \mathbf{v}\cdot\nabla\varphi(\mathbf{r}, t) - \frac{\partial}{\partial t}\varphi(\mathbf{r}, t) = 0 \qquad (10)$$

where $\mathbf{r} = (x, y)$ the spatial coordinates, D the diffusion coefficient, $\mathbf{v}$ the advection velocity. Taking a Fourier transform with respect to $\mathbf{r}$, we obtain the expression in frequency domain ($\mathbf{q}$),

$$\left(-Dq^2 + i\mathbf{q}\cdot\mathbf{v} - \frac{\partial}{\partial t}\right)\varphi(\mathbf{q}, t) = 0. \qquad (11)$$

In Eq. 11, the same symbols with different argument are used to present a function and its Fourier transform, i.e., $f(\mathbf{r}) \leftrightarrow$
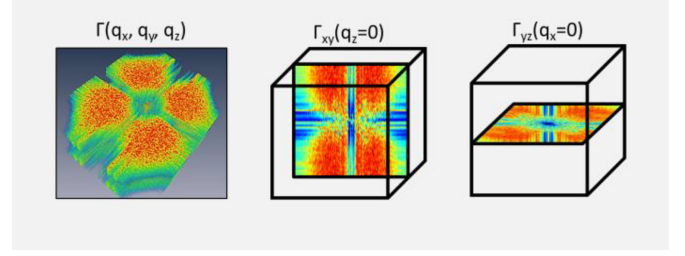
Fig. 9. 3D intracellular transport using DPS. Using time-lapse tomograms, one can calculate the dispersion-relation on both x-y and y-z plane, and, then 3D diffusion and advection bandwidth are retrieved. Adapted with permission from Ref. [50].

$f(\mathbf{q})$, where f is an arbitrary signal and $\leftrightarrow$ indicates the Fourier transform. The Fourier transform of the input phase stack is shown in Fig. 8c. The temporal autocorrelation at each spatial frequency (i.e., transport along a certain direction), g(q,t), can be described as

$$g(q, t) = e^{iv_0 qt}e^{-q\Delta vt - Dq^2 t} \qquad (12)$$

where v_0 represents the mean velocity, and Δv the bandwidth of the deterministic velocity. For most cases, we found that v_0 is negligibly small, meaning that the intracellular mass transport is equally probable in all directions. Then, the exponential decay rate, at each spatial frequency, $\Gamma(q)$, is expressed as,

$$\Gamma(q) = Dq^2 + \Delta vq. \qquad (13)$$

And Γ can be calculated to be the standard deviation of the spatial power spectrum (Fig. 8d). A radial average is followed to reduce the 2D map into a 1D line profile (Fig. 8e). The Δv and D values are then extracted by fitting the data to Eq. 13.

More recently, Kandel *et al.* showed that, by feeding time-lapse tomograms to the DPS method, one can investigate mass transport in both transverse and axial directions (Fig. 9) [50].

Microtubules, which are important components of cytoskeleton, have a tubular structure typically with an outer diameter around 24 nm and inner diameter about 12 nm, and it can grow as long as 50 μm [51]. These tiny structures play an active role in intracellular transport as well as many other cellular processes [52], [53]. However, the extreme small dimension of a single microtubule makes it difficult to be resolved by a conventional far-field microscope. In Ref. [54], the authors successfully demonstrated the capability of imaging single microtubule *in vitro* using SLIM. Though the resolving power of microscope is still limited by the diffraction limit, its sub-nanometer sensitivity and stability make it possible to capture the phase shift introduced by ting objects. According to their measurement, a single microtubule yields a phase shift in the order of 1 mrad, corresponding to a refractive index of 1.475. Because SLIM does not require external labeling, the image stayed the same level of contrast after 3 minutes of the measurement, while the fluorescent signal faded away due to photobleaching (Fig. 10). More importantly, they applied DPS calculation to every 128 frames, roughly 400 ms, and studied the change of velocity bandwidth in a period of 2 hours, where a decreased motility
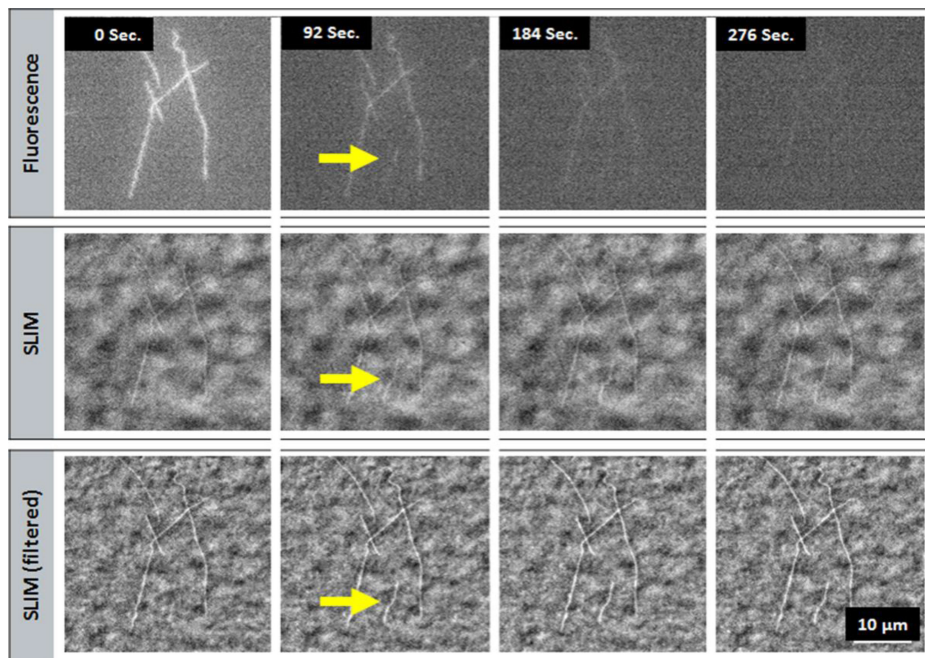
Fig. 10. SLIM enables continuous observation of microtubules without photobleaching. (top row) Fluorescence microscopy image, using the HiLyte 488 dye. Note that a descending microtubule is not visible due to photobleaching (arrow). (middle row) SLIM images of the same field of view. (bottom row) For easier visualization, the SLIM sequence was filtered with a spatial high-pass filter, displayed in the same gray scale. Adapted with permission from Ref. [54].

was observed. Clearly, this exceptional conclusion cannot be obtained from conventional imaging methods.

C. Optogenetics

Optogenetics is a transformational method for studying functions of neural network [55]. Through gene engineering, a cell can produce light sensitive proteins, and as a result, its activities can be manipulated by light. Unlike conventional electrical stimulation, light can be precisely delivered to some group or specific types of neurons in a network, and this mechanism makes it possible to investigate the impact of subpopulation neurons on a neural circuit [56]. QPI, as well as some other interferometric methods, measure the phase shift in high sensitivity, which would enable label-free investigation of stimulated neuro dynamics at a large spatial scale [57]–[59].

In authors' lab, the cellular dynamics within optogenetically activated PC-12 derived neuron cultures transfected with *Channelrhodopsin* 2 (ChR2) were recently investigated [15]. Once these transfected neuron like cells are exposed to blue light, protein channels on the cell membrane would open, which allows positive ions to enter the cell from the extracellular medium [60]. The sudden influx of positive ions depolarizes the cell, and this can trigger action potentials and also cause transport of various cellular organelles. A DPM system coupled with a projector was built to achieve programmable sub-cellular optogenetic excitation and label-free imaging. For individual transfected cell, an active stimulation light (blue) for 3 seconds was applied, then phase imaging followed for 3 minutes. This measurement was repeated under a negative stimulation (red) and no stimulation condition. For control, non-transfected neuron under the same stimulation conditions were conducted. Fig. 11
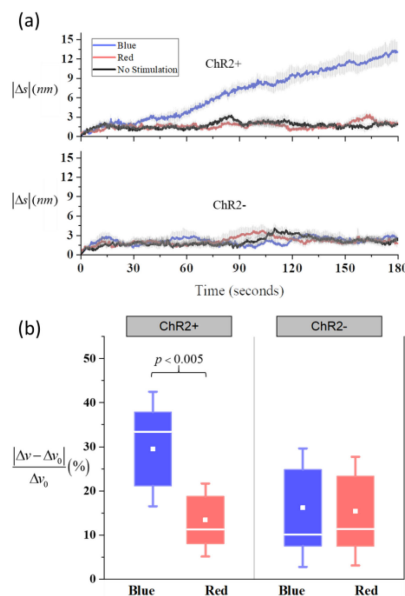
Fig. 11. Optogenetically activated neuronal activities. (a) Optical pathlength (OPL) change after applying different stimulation conditions on both ChR2+ and ChR2- neurons at subcellular regions. All ROIs were located either on neuron dendrites, axon, or the region of cellbody close to a dendrite. The absolute change of averaged phase with respect to t = 0 were plotted for each stimulation condition, with standard errors indicated by light-gray bars. (b) Using DPS, a box chart was obtained, which plotting the transport velocity change compared with the velocity under no light stimulation after different stimulation on ChR2+ and ChR2- (unit in %). Adapted with permission from Ref. [15].

shows the magnitude of optical pathlength change, which is essentially proportional to dry mass, in selected dendritic regions. Moreover, the DPS results indicates drastic changes in ChR2+
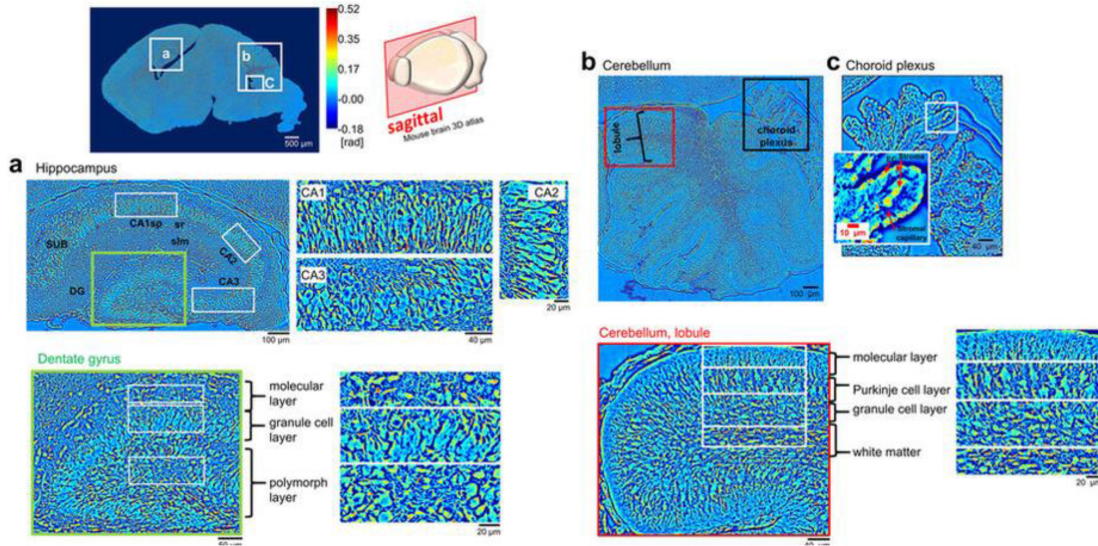
Fig. 12. A brain slice imaging by a QPI tissue scanner. Regions (a) hippocampus, (b) cerebellum and (c) choroid plexus are shown at increasing magnification. The green box in (a) shows the area of the dentate gyrus. The red box in (b) shows a cerebellum lobule. The layered structure for each region is analyzed in terms of phase value. The red arrows in (c) are pointing to stromal capillaries within the choroid plexus. Adapted with permission from Ref. [66].

cell when received active stimulation, which suggest an enhanced cellular traffic recorded by phase measurement.

D. Pathological Applications

Histology is considered the 'gold standard' to study tissue organization and alterations associated with diseases. The traditional histological methods use various stains to render colors at different tissue structures, but this only provides qualitative information and the staining outcome varies between cases [61]. QPI tissue scanner, however, doesn't require tissue staining, and its full field imaging capability would achieve an acquisition rate as fast as the conventional tissue scanner. More importantly, the intrinsic phase contrast would pick up structures that cannot be observed in stained tissue due to staining error. In the past, QPI have demonstrated to be useful to diagnose anomalies in a few types of tissues [62]–[64]. In more recent studies, QPI also shows the potential of studying morphological changes associated with neurological disorders.

At cellular level, QPI allows quantitatively monitoring morphology and biomolecule alterations in cells to study pathophysiology. For instance, Yang *et al.* measured the individual neurons using 3D optical diffraction tomography (ODT) to investigate the early neurotoxic effect *in vitro* Parkinson's disease (PD) model [65]. In this experiment, after 5 hours of treatment with chemical caused PD like symptoms, apoptotic features were found in effected cells.

At tissue level study, by incorporating a motorized stage to a SLIM system, Min *et al.* demonstrated the principle of mapping morphology of brain slices [66]. In this research, segmented phase images were acquired with high resolution, and then digitally stitched to generate the whole view of brain slices of mice (Fig. 12). As one can see, anatomical structures, such as hippocampus, cerebellum and choroid plexus, are delineated in detail across specimen without necessity of staining.

In addition, other than the quantitative phase value, one can study tissue's scattering properties to interpret its organization. Scattering-phase theorem [67] maps the phase image of a thin tissue slice in terms of scattering mean free path, l_s, and the anisotropy factor, g, which are two parameters related to the scattering properties of the measured specimen. l_s is the mean distance travelled by light for a single scattering event, and g is the average cosine of the scattering angle over a tissue thickness equal to l_s. Using $l_s - g$ relation, one can distinguish tissue architecture, study the changes in tissue organization due to injury, and realize diagnosis purpose [68], [69]. Both l_s and g can be extracted from a measured phase map,

$$l_s = \frac{L}{\langle \Delta \phi^2 (r) \rangle} \quad (14)$$

$$g = 1 - \left(\frac{l_s}{L}\right)^2 \frac{\langle |\nabla \varphi (r)|^2 \rangle}{2k_0^2} \quad (15)$$

where L is the thickness of tissue slice (typically between 3-5 μm), $\langle \Delta \phi^2(r) \rangle$ is the spatial variance of φ over a certain window, $k_0 = 2\pi n_0/\lambda$, λ the central wavelength, n_0 the refractive index of the tissue, and $\langle |\nabla \varphi(r)|^2 \rangle$ is the spatial average of the square magnitude of the gradient phase.

In Ref. [70], Lee *et al.* developed a DPM-based tissue scanner to study Alzheimer's disease (AD) affected brain slices. By using scattering-phase theorem, they retrieved maps of scattering coefficient (u_s), essentially the reciprocal of l_s, and anisotropy (g). In u_s and g maps, some important brain architecture, such as grey, white matter, hippocampus, are clearly separated. Furthermore, by comparing l_s and g at different regions between normal and mice with AD, authors found a higher inhomogeneity and increased size of scattering particles in the grey and hippocampal regions in AD effected tissues.

V. Summary and Future Direction

Quantitative phase imaging is a label-free modality suitable for studying both fixed and live biological samples. Exploiting the principle of interferometry, QPI measures the optical pathlength difference with sub-nanometer scale sensitivity and stability. In the past decades, a number of QPI systems were invented, which enables different experiments performed at various temporal and spatial scale. Temporally, since no exogenous labeling is needed, QPI enables measuring dynamics phenomena from the millisecond scale, to days, even weeks long processes. Spatially, QPI also caters to different needs, ranging from detecting tiny subcellular structures with dimensions below the resolution limit, to mapping the morphology of whole tissue slices. During the process of enriching QPI imaging platforms, numerical analysis methods were developed as complementary tools to extract either functional or structural knowledge of the studied object. Through the exemplary studies shown in here, one can see that QPI has become a remarkable tool for biomedical applications, and, specifically, neuroscience. Though tremendous progress has been achieved so far, it still faces a few challenges. (1) "Optophysiology", by which one measures the changes in optical properties associated with an action potential in a single mammalian neuron, has not been fully demonstrated yet. The traditional electrophysiology methods, potentially invasive and requiring contact, are still considered the 'gold standard' in neuroscience. Even though a few publications prove that QPI provides enough sensitivity to detect phase change related to membrane potential [71], or read out subtle activities due to stimulation, no single action potential or calcium signal has been isolated so far from the phase response. (2) If one is interested in a specific component within the specimen, QPI still relies on other methods, such as fluorescent imaging, for validation. One proposed solution is letting scattering particles, such as high refractive index nanoparticles or gas vesicles, fuse with structures of interest, which would boost the phase response at the specified region. This way, one would obtain highly specific measurements, without limitations associated with photobleaching and photoxicity. However, question arises as to whether adding external agents would impact the viability in live samples. (3) Compared to the high speed data production in QPI experiments, the efficiency of data analysis is relatively low. Though some image processing algorithms, such as NeuronJ, would automatically segment or trace certain features, manual or semi-manual selection is still needed and even repeated frame by frame [72]. With the concomitant progress in the computational areas [73, 74], especially artificial intelligence algorithms, we expect to see a continuously growing QPI field, valuable to the broad neuroscience community.

References

[1] G. Popescu, *Quantitative Phase Imaging of Cells and Tissues*. New York, NY, USA: McGraw-Hill, 2011.

[2] F. Zernike, "Phase contrast, a new method for the microscopic observation of transparent objects Part II," (in English), *Physica*, vol. 9, pp. 974–986, 1942.

[3] J. Mertz, *Introduction to Optical Microscopy*. WI, USA: Roberts, 2010.

[4] D. Gabor, "A new microscopic principle," (in English), *Nature*, vol. 161, no. 4098, pp. 777–778, 1948.

[5] R. Collier, *Optical Holography*. Amsterdam, The Netherlands: Elsevier, 2013.

[6] P. Marquet *et al.*, "Digital holographic microscopy: A noninvasive contrast imaging technique allowing quantitative visualization of living cells with subwavelength axial accuracy," (in English), *Opt. Lett.*, vol. 30, no. 5, pp. 468–470, Mar. 2005.

[7] K. Lee *et al.*, "Quantitative phase imaging techniques for the study of cell pathophysiology: From principles to applications," *Sensors (Basel)*, vol. 13, no. 4, pp. 4170–4191, Mar. 2013.

[8] D. Jin, R. J. Zhou, Z. Yaqoob, and P. T. C. So, "Tomographic phase microscopy: Principles and applications in bioimaging [Invited]," (in English), *J. Opt. Soc. Amer. B Opt. Phys.*, vol. 34, no. 5, pp. B64–B77, May 2017.

[9] S. Chowdhury, W. J. Eldridge, A. Wax, and J. A. Izatt, "Structured illumination multimodal 3D-resolved quantitative phase and fluorescence sub-diffraction microscopy," *Biomed. Opt. Express*, vol. 8, no. 5, pp. 2496–2518, May 2017.

[10] N. T. Shaked, L. L. Satterwhite, M. T. Rinehart, and A. Wax, "Quantitative analysis of biological cells using digital holographic microscopy," (in English), *Holography, Res. Technol.*, pp. 219–236, 2011.

[11] W. Choi *et al.*, "Tomographic phase microscopy," (in English), *Nature Methods*, vol. 4, no. 9, pp. 717–719, Sep. 2007.

[12] C. Hu and G. Popescu, "Physical significance of backscattering phase measurements," *Opt. Lett.*, vol. 42, no. 22, pp. 4643–4646, 2017.

[13] G. Popescu, T. Ikeda, R. R. Dasari, and M. S. Feld, "Diffraction phase microscopy for quantifying cell structure and dynamics," *Opt. Lett.*, vol. 31, no. 6, pp. 775–777, Mar. 2006.

[14] B. Bhaduri *et al.*, "Diffraction phase microscopy: Principles and applications in materials and life sciences," (in English), *Adv. Opt. Photon.*, vol. 6, no. 1, pp. 57–119, Mar. 2014.

[15] C. Hu *et al.*, "Optical excitation and detection of neuronal activity," arXiv:1711.02177, 2017.

[16] H. V. Pham, C. Edwards, L. L. Goddard, and G. Popescu, "Fast phase reconstruction in white light diffraction phase microscopy," *Appl. Opt.*, vol. 52, no. 1, pp. A97–101, Jan. 2013.

[17] C. Edwards, B. Bhaduri, B. G. Griffin, L. L. Goddard, and G. Popescu, "Epi-illumination diffraction phase microscopy with white light," *Opt. Lett.*, vol. 39, no. 21, pp. 6162–5, Nov. 2014.

[18] M. Finkeldey, L. Goring, C. Brenner, M. Hofmann, and N. C. Gerhardt, "Depth-filtering in common-path digital holographic microscopy," *Opt. Express*, vol. 25, no. 16, pp. 19398–19407, Aug. 2017.

[19] C. Hu, S. Zhu, L. Gao, and G. Popescu, "Endoscopic diffraction phase microscopy," *Opt. Lett.*, vol. 43, no. 14, pp. 3373–3376, Jul. 2018.

[20] H. Pham, B. Bhaduri, H. Ding, and G. Popescu, "Spectroscopic diffraction phase microscopy," *Opt. Lett.*, vol. 37, no. 16, pp. 3438–40, Aug. 2012.

[21] E. Min *et al.*, "Measurement of multispectral scattering properties in mouse brain tissue," *Biomed. Opt. Express*, vol. 8, no. 3, pp. 1763–1770, Mar. 2017.

[22] J. Jung *et al.*, "Biomedical applications of holographic microspectroscopy [invited]," *Appl. Opt.*, vol. 53, no. 27, pp. G111–G122, Sep. 2014.

[23] H. Majeed *et al.*, "Magnified image spatial spectrum (MISS) microscopy for nanometer and millisecond scale label-free imaging," *Opt. Express*, vol. 26, no. 5, pp. 5423–5440, Mar. 2018.

[24] Z. Wang *et al.*, "Spatial light interference microscopy (SLIM)," *Opt. Express*, vol. 19, no. 2, pp. 1016–1026, Jan. 2011.

[25] T. Kim *et al.*, "White-light diffraction tomography of unlabelled live cells," *Nature Photon.*, vol. 8, no. 3, pp. 256–263, 2014.

[26] P. Cintora, J. Arikkath, M. Kandel, G. Popescu, and C. Best-Popescu, "Cell density modulates intracellular mass transport in neural networks," *Cytometry A*, vol. 91, no. 5, pp. 503–509, May 2017.

[27] T. H. Nguyen, M. E. Kandel, M. Rubessa, M. B. Wheeler, and G. Popescu, "Gradient light interference microscopy for 3D imaging of unlabeled specimens," *Nature Commun.*, vol. 8, no. 1, Aug. 2017, Art. no. 210.

[28] B. Kemper and G. von Bally, "Digital holographic microscopy for live cell applications and technical inspection," (in English), *Appl. Opt.*, vol. 47, no. 4, pp. A52–A61, Feb. 2008.

[29] F. Merola *et al.*, "Tomographic flow cytometry by digital holography," (in English), *Light, Sci. Appl.*, vol. 6, Apr. 2017, Art. no. e16241.

[30] M. Mir *et al.*, "Optical measurement of cycle-dependent cell growth," *Proc. Nat. Acad. Sci. USA*, vol. 108, no. 32, pp. 13124–13129, Aug. 2011.

[31] Y. Park *et al.*, "Measurement of red blood cell mechanics during morphological changes," *Proc. Nat. Acad. Sci. USA*, vol. 107, no. 15, pp. 6731–6736, Apr. 2010.

[32] N. T. Shaked, J. D. Finan, F. Guilak, and A. Wax, "Quantitative phase microscopy of articular chondrocyte dynamics by wide-field digital interferometry," *J. Biomed. Opt.*, vol. 15, no. 1, Jan./Feb. 2010, Art. no. 010505.

[33] R. Wang *et al.*, "One-dimensional deterministic transport in neurons measured by dispersion-relation phase spectroscopy," (in English), *J. Phys.-Condens. Matter*, vol. 23, no. 37, Sep. 2011, Art. no. 374107.

[34] B. Mandracchia, O. Gennari, A. Bramanti, S. Grilli, and P. Ferraro, "Label-free quantification of the effects of lithium niobate polarization on cell adhesion via holographic microscopy," *J. Biophoton.*, vol. 11, Feb. 2018, Art. no. e201700332.

[35] A. Calabuig, M. Mugnano, L. Miccio, S. Grilli, and P. Ferraro, "Investigating fibroblast cells under "safe" and "injurious" blue-light exposure by holographic microscopy," *J. Biophoton.*, vol. 10, no. 6/7, pp. 919–927, Jun. 2017.

[36] W. J. Eldridge, Z. A. Steelman, B. Loomis, and A. Wax, "Optical phase measurements of disorder strength link microstructure to cell stiffness," *Biophys. J.*, vol. 112, no. 4, pp. 692–702, Feb. 2017.

[37] M. T. Rinehart, H. S. Park, K. A. Walzer, J. T. Chi, and A. Wax, "Hemoglobin consumption by *P. falciparum* in individual erythrocytes imaged via quantitative phase spectroscopy," *Sci. Rep.*, vol. 6, Apr. 2016, Art. no. 24461.

[38] H. V. Pham, B. Bhaduri, K. Tangella, C. Best-Popescu, and G. Popescu, "Real time blood testing using quantitative phase imaging," (in English), *Plos One*, vol. 8, no. 2, Feb. 2013, Art. no. e55676.

[39] M. Ogawa *et al.*, "Immunogenic cancer cell death selectively induced by near infrared photoimmunotherapy initiates host tumor immunity," (in English), *Oncotarget*, vol. 8, no. 6, pp. 10425–10436, Feb. 2017.

[40] H. Majeed *et al.*, "Quantitative phase imaging for medical diagnosis," *J. Biophoton.*, vol. 10, no. 2, pp. 177–205, Feb. 2017.

[41] P. Marquet, C. Depeursinge, and P. J. Magistretti, "Review of quantitative phase-digital holographic microscopy: Promising novel imaging technique to resolve neuronal network activity and identify cellular biomarkers of psychiatric disorders," *Neurophotonics*, vol. 1, no. 2, Oct. 2014, Art. no. 020901.

[42] J. A. Cardin *et al.*, "Targeted optogenetic stimulation and recording of neurons in vivo using cell-type-specific expression of Channelrhodopsin-2," *Nature Protocols* vol. 5, no. 2, pp. 247–254, 2010, doi: 10.1038/nprot.2009.228.

[43] J. Akerboom *et al.*, "Genetically encoded calcium indicators for multi-color neural activity imaging and combination with optogenetics," *Front. Mol. Neurosci.*, vol. 6, pp. 2–30, 2013.

[44] Z. V. Guo, A. C. Hart, and S. Ramanathan, "Optical interrogation of neural circuits in Caenorhabditis elegans," *Nature Methods*, vol. 6, no. 12, pp. 891–896, Dec. 2009.

[45] Y. Y. Gong *et al.*, "High-speed recording of neural spikes in awake mice and flies with a fluorescent voltage sensor," (in English), *Science*, vol. 350, no. 6266, pp. 1361–1366, Dec. 2015.

[46] E. C. Jensen, "Use of fluorescent probes: Their effect on cell biology and limitations," (in English), *Anatomical Record-Adv. Integrative Anatomy Evolutionary Biol.*, vol. 295, no. 12, pp. 2031–2036, Dec. 2012.

[47] G. Popescu *et al.*, "Optical imaging of cell mass and growth dynamics," *Amer. J. Physiol. Cell Physiol.*, vol. 295, no. 2, pp. C538–C544, Aug. 2008.

[48] M. Mir *et al.*, "Label-free characterization of emerging human neuronal networks," *Sci. Rep.*, vol. 4, Mar. 2014, Art. no. 4434.

[49] R. Wang *et al.*, "Dispersion-relation phase spectroscopy of intracellular transport," *Opt. Express*, vol. 19, no. 21, pp. 20571–20579, Oct. 2011.

[50] M. E. Kandel *et al.*, "Three-dimensional intracellular transport in neuron bodies and neurites investigated by label-free dispersion-relation phase spectroscopy," *Cytometry A*, vol. 91, no. 5, pp. 519–526, May 2017.

[51] D. Bermudes, G. Hinkle, and L. Margulis, "Do prokaryotes contain microtubules," (in English), *Microbiol. Rev.*, vol. 58, no. 3, pp. 387–400, Sep. 1994.

[52] N. Okada and M. Sato, "Spatiotemporal regulation of nuclear transport machinery and microtubule organization," *Cells*, vol. 4, no. 3, pp. 406–426, Aug. 2015.

[53] I. M. Kulic *et al.*, "The role of microtubule movement in bidirectional organelle transport," *Proc. Nat. Acad. Sci. USA*, vol. 105, no. 29, pp. 10011–10016, Jul. 2008.

[54] M. E. Kandel, K. W. Teng, P. R. Selvin, and G. Popescu, "Label-free imaging of single microtubule dynamics using spatial light interference microscopy," (in English), *ACS Nano*, vol. 11, no. 1, pp. 647–655, Jan. 2017.

[55] L. Fenno, O. Yizhar, and K. Deisseroth, "The development and application of optogenetics," *Annu. Rev. Neurosci.*, vol. 34, pp. 389–412, 2011.

[56] A. M. Packer, B. Roska, and M. Hausser, "Targeting neurons and photons for optogenetics," *Nature Neurosci.*, vol. 16, no. 7, pp. 805–15, Jul. 2013.

[57] P. Marquet, C. Depeursinge, and P. J. Magistretti, "Exploring neural cell dynamics with digital holographic microscopy," *Annu. Rev. Biomed. Eng.*, vol. 15, pp. 407–31, 2013.

[58] S. Batabyal *et al.*, "Label-free optical detection of action potential in mammalian neurons," *Biomed. Opt. Express*, vol. 8, no. 8, pp. 3700–3713, Aug. 2017.

[59] B. W. Graf, T. S. Ralston, H. J. Ko, and S. A. Boppart, "Detecting intrinsic scattering changes correlated to neuron action potentials using optical coherence imaging," (in English), *Opt. Express*, vol. 17, no. 16, pp. 13447–13457, Aug. 2009.

[60] O. Yizhar, L. E. Fenno, T. J. Davidson, M. Mogri, and K. Deisseroth, "Optogenetics in neural systems," *Neuron*, vol. 71, no. 1, pp. 9–34, Jul. 2011.

[61] Taylor, C. R., and R. M. Levenson. "Quantification of immunohistochemistry-issues concerning methods, utility and semi-quantitative assessment II." *Histopathology* 49, no. 4 pp. 411–424, 2006.

[62] H. Majeed *et al.*, "Breast cancer diagnosis using spatial light interference microscopy," (in English), *J. Biomed. Opt.*, vol. 20, no. 11, Nov. 2015, Art. no. 111210.

[63] H. Ding *et al.*, "Measuring the scattering parameters of tissues from quantitative phase imaging of thin slices," *Opt. Lett.*, vol. 36, no. 12, pp. 2281–2283, Jun. 2011.

[64] M. E. Kandel *et al.*, "Label-free tissue scanner for colorectal cancer screening," *J. Biomed. Opt.*, vol. 22, no. 6, Jun. 2017, Art. no. 66016.

[65] S. A. Yang, J. Yoon, K. Kim, and Y. Park, "Measurements of morphological and biophysical alterations in individual neuron cells associated with early neurotoxic effects in parkinson's disease," (in English), *Cytometry Part A*, vol. 91a, no. 5, pp. 510–518, May 2017.

[66] E. Min *et al.*, "Label-free, multi-scale imaging of ex-vivo mouse brain using spatial light interference microscopy," *Sci. Rep.*, vol. 6, Dec. 2016, Art. no. 39667.

[67] Z. Wang, H. Ding, and G. Popescu, "Scattering-phase theorem," *Opt. Lett.*, vol. 36, no. 7, pp. 1215–1217, Apr. 2011.

[68] S. Ban *et al.*, "Optical properties of acute kidney injury measured by quantitative phase imaging," *Biomed. Opt. Express*, vol. 9, no. 3, pp. 921–932, Mar. 2018.

[69] S. Sridharan, V. Macias, K. Tangella, A. Kajdacsy-Balla, and G. Popescu, "Prediction of prostate cancer recurrence using quantitative phase imaging," (in English), *Sci. Rep.*, vol. 5, May 2015, Art. no. 9976.

[70] M. Lee *et al.*, "Label-free optical quantification of structural alterations in Alzheimer's disease," *Sci. Rep.*, vol. 6, 2016, Art. no. 31034.

[71] S. Oh *et al.*, "Label-free imaging of membrane potential using membrane electromotility," (in English), *Biophys. J.*, vol. 103, no. 1, pp. 11–18, Jul. 2012.

[72] Y. J. Lee *et al.*, "Quantitative assessment of neural outgrowth using spatial light interference microscopy," (in English), *J. Biomed. Opt.*, vol. 22, no. 6, Jun. 2017, Art. no. 66015.

[73] Y. Jo *et al.*, "Holographic deep learning for rapid optical screening of anthrax spores," *Sci. Adv.*, vol. 3, no. 8, Aug. 2017, Art. no. e1700606.

[74] H. S. Park, M. Rinehart, K. A. Walzer, J. T. A. Chi, and A. Wax, "Automated detection of *P. falciparum* using machine learning algorithms with quantitative phase images of unstained cells," (in English), *Plos One*, vol. 11, no. 9, Sep. 2016, Art. no. e0163045.

Chenfei Hu is currently working toward the Ph.D. degree in electrical and computer engineering at University of Illinois at Urbana-Champaign (UIUC), Champaign, IL, USA. In 2016, he joined Quantitative Light Imaging (QLI) Laboratory, Beckman Institute for Advanced Science and Technology. His research interests include developing quantitative phase imaging (QPI) platforms, designing computational data analyzing methods, and applying these techniques to biomedical applications.

Gabriel Popescu is currently a Professor in electrical and computer engineering at UIUC. His research is focused on biomedical optics and quantitative phase imaging (QPI) of cells and tissue. So far, he has published a book on QPI, authored more than 150 journal publications, and 200 conference presentations, authored 29 issued and pending patents, and given 185 invited/keynote/plenary talks. He founded Phi Optics, Inc., a startup company that commercializes quantitative phase imaging technology. He is a fellow of OSA and SPIE.